Supplementary Materials

Implied timescales

We built our Markov state models using the discretization discovered by the khybrid clustering algorithm on SASA feature vectors (see Methods). We then verified our choice of kcenters stopping condition (2.6 nm^2 for TEM-1 and 3.0 nm^2 for CTX-M-9) and chose our lag times (4 ns for TEM-1 and 0.6 ns for CTX-M-9) using the implied timescales test.

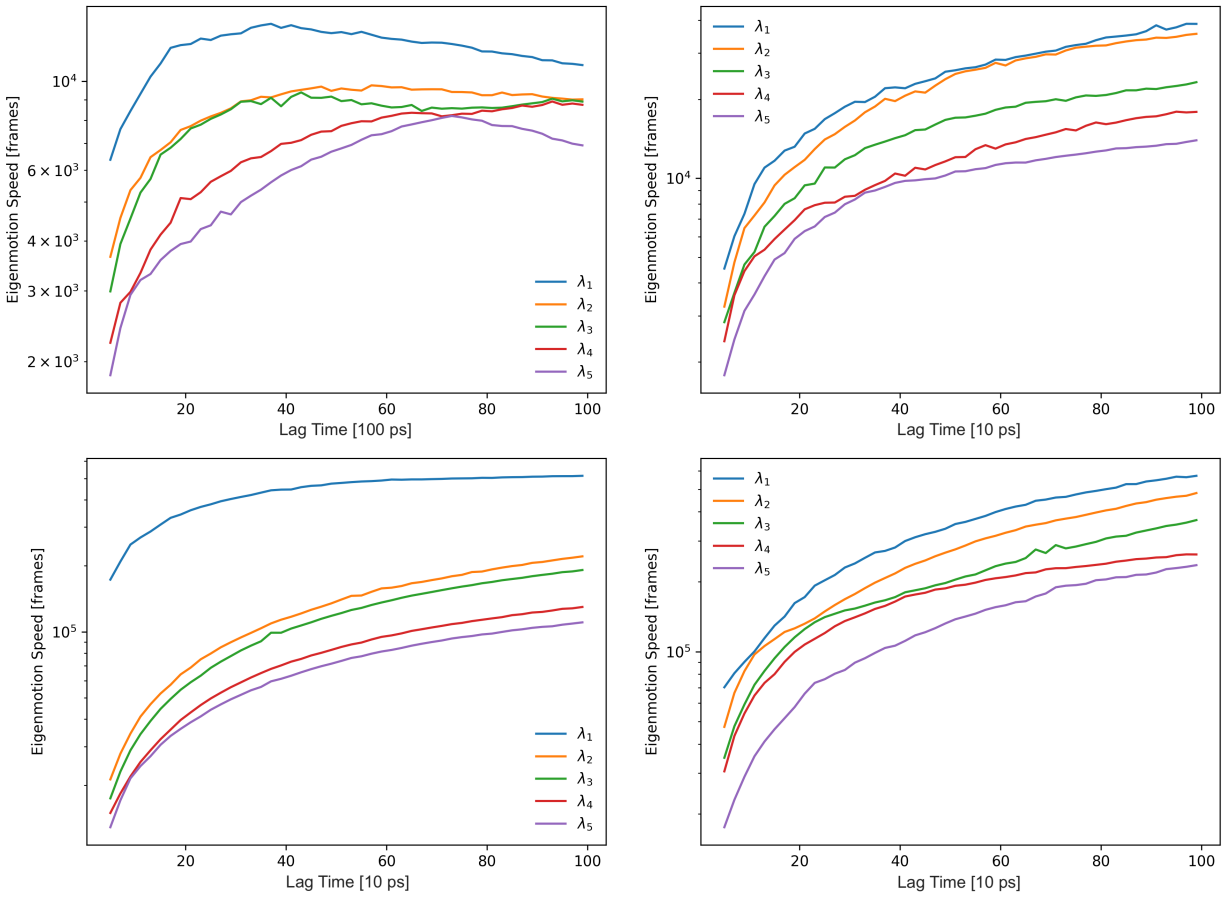

Figure S1: Implied timescales tests for TEM-1 (top left), CTX-M-9 (top right), CAP (bottom left), and eNP (bottom right). The implied timescales test is a test for Markovianity of an MSM. The model is fit with a variety of lag times (x-axis) and the slowest few motions' speed is computed. In a good model, the timescales are relatively insensitive to lag time, and so typically a lag time will be chosen that minimizes the derivative of implied timescale with respect to lag time. (1, 2)

Affinity clustering is stable to damping parameter changes

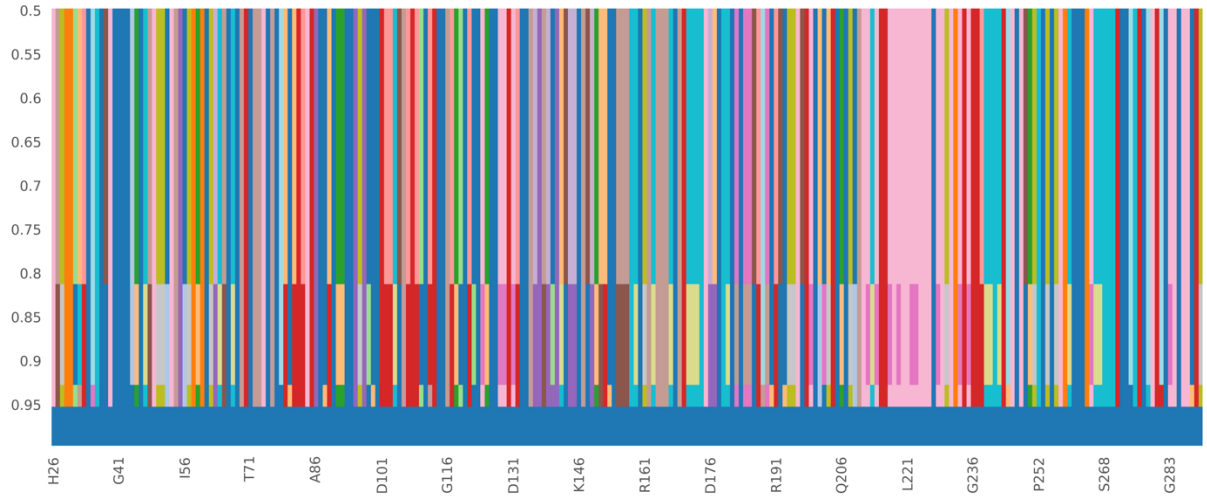

Figure S2: Affinity clustering is stable across most values of the damping parameter in TEM-1. This figure is a parameter scan across the range of possible damping parameters for the clustering algorithm that assigns residues to exposons. In this figure, the y-axis represents choice of damping parameter, the x-axis represents the protein sequence. The color of at any position denotes the exposon to which a residue was assigned at that particular choice of damping parameter. Thus, the appearance of vertical bars is a consequence of the fact that residues generally do not change which exposon they are assigned to. Some residues are assigned to the same cluster for all damping parameter choices < 0.95.

Time-resolved DTNB thiol labeling by stopped-flow

To measure the labeling rate of any particular residue, we prepared the relevant cysteine mutant (see *Methods*) and ran triplicate DNTB labeling experiments both with and without protein. We subtracted the baseline absorbance of DTNB in buffer from the labeling trace and fit to a single exponential. Each point in Fig 2b and e represents the results of such a procedure. A representative fit to the data for TEM-1 at 500 μM DTNB is shown below.

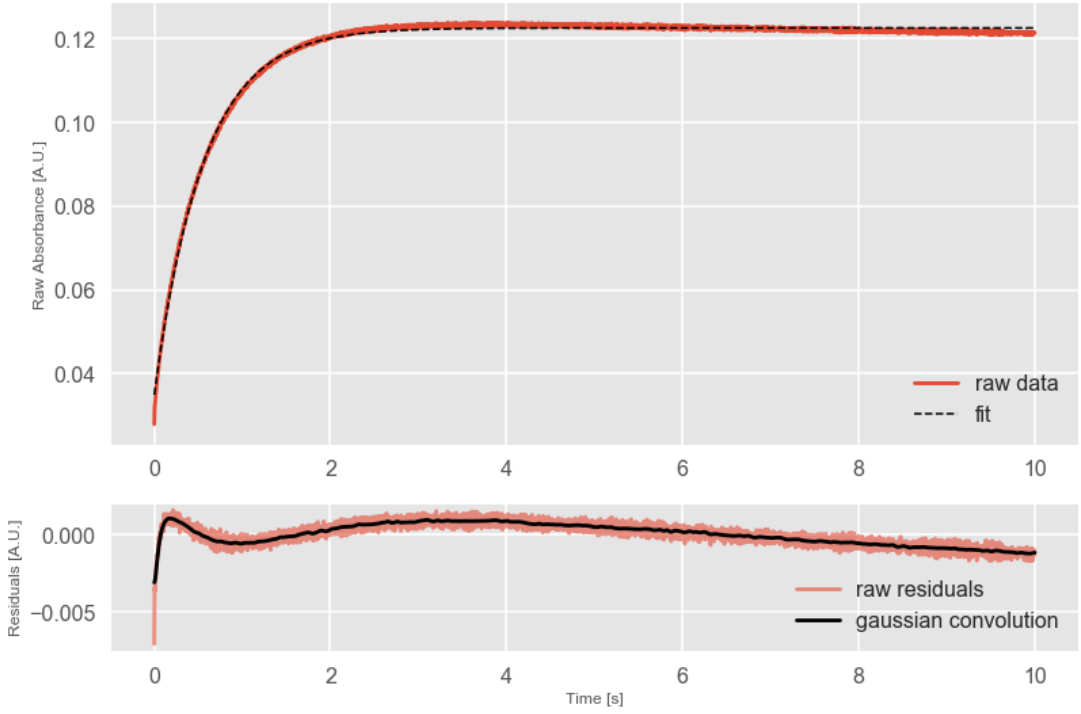

Fig S3: A representative trace of absorbance over time for a sample of 9 μM TEM-1 S243C mixed with 500 μM DTNB along with a single exponential fit (top) and the residuals to that same model (bottom). For the top figure, red is raw data and dashed black is the fit. For the bottom figure, red represents the raw residuals and black represents a Gaussian convolution of that data.

Table S1. Parameters of Linderstrøm-Lang model of DTNB labeling. Error is the standard deviation from 100 trials of bootstrapping.

	TEM-1 M182T S243C	*CTX-M-9*
k_{int}	6.83 ± 1.18 mM^{-1} s^{-1}	71.5 ± 5.3 mM^{-1} s^{-1}
K	1.10 x 10^{-2} ± 1.9 x 10^{-3}	2.34 x 10^{-4} ± 7.8 x 10^{-5}
k_{op}	N/A	1.22 x 10^{-2} ± 2.05 x 10^{-3} s^{-1}
k_{cl}	N/A	51.3 ± 14.4 s^{-1}
$K \times k_{\text{int}}$	7.5 x 10^{-2} ± 1.5 x 10^{-3} mM^{-1} s^{-1}	1.67 x 10^{-2} ± 5.70 x 10^{-3} mM^{-1} s^{-1}

Estimation of global unfolding rates of TEM-1 S243C and CTX-M-9

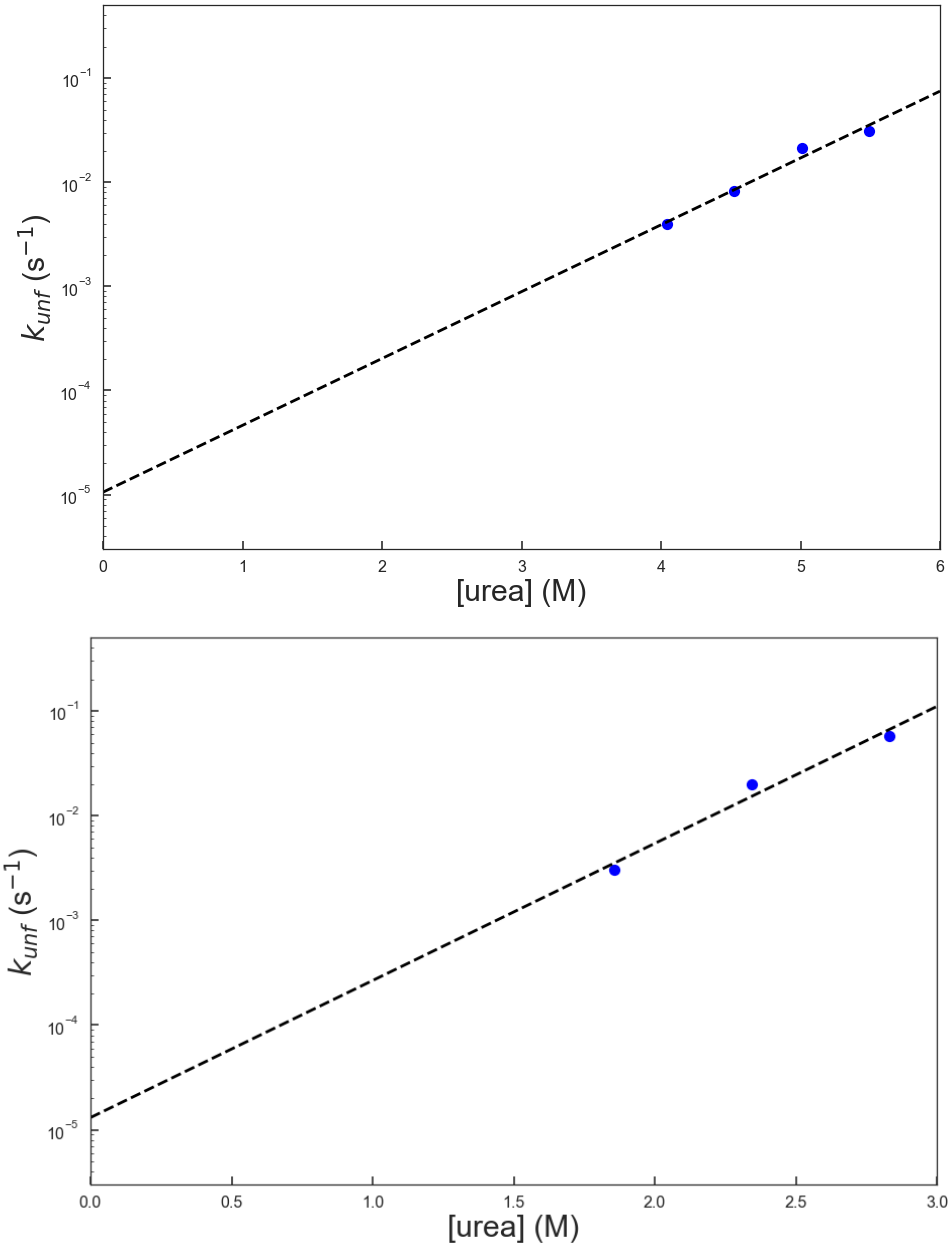

Fig S4: Rates of unfolding of TEM-1 S243C (top) and CTX-M-9 (bottom) as a function of urea concentration. A linear fit is used to extrapolate to the rate of global unfolding of each protein to the rate in the absence of urea. The rate of unfolding for TEM-1 S234C is $1.054 \times 10^{-5} \pm 1.371 \times 10^{-5}$ s^{-1} whereas the rate of unfolding for CTX-M-9 is $1.308 \times 10^{-5} \pm 2.274 \times 10^{-5}$ s^{-1}. Error is estimated using the standard deviation from 100 rounds of bootstrapping.

Protein stability measurements

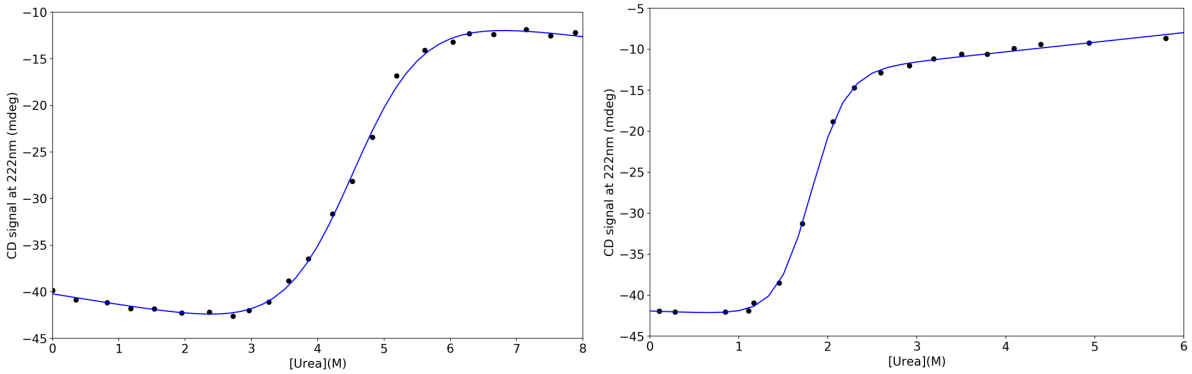

Fig S5: Circular dichroism as a function of urea concentration (solid circles) fit to a two-state model (equation S1) of unfolding for TEM-1 S243C (left) and CTX-M-9 (right). Data were collected in triplicate.

$$(1)\ \mathrm{CD}\ (\Theta) = \frac{\Theta_u + \Theta_n e^{-(\Delta G_{un} + m_{un}[\mathrm{urea}])/RT}}{1 + e^{-(\Delta G_{un} + m_{un}[\mathrm{urea}])/RT}}$$

where Θ_u and Θ_n are the Circular Dichroism signals at 222 nm for the unfolded and native states. ΔG_{un} is the extrapolated free energy change in 0 M urea between the unfolded and native states, and m_{un} is a proportionality term related to the steepness of the linear fit of the unfolded to native state transition (3).

Table S2. Equilibrium Fit Parameters. Errors are standard deviations.

	ΔG_{un} (kcal mol^{-1})	m_{un} (kcal mol^{-1} M^{-1})	C_m (M)
TEM-1 M182T S243C	5.0 ± 0.3	1.12 ± 0.07	4.5 ± 0.4
CTX-M-9	5.5 ± 0.2	3.0 ± 0.1	1.83 ± 0.09

Activity of labeled enzyme

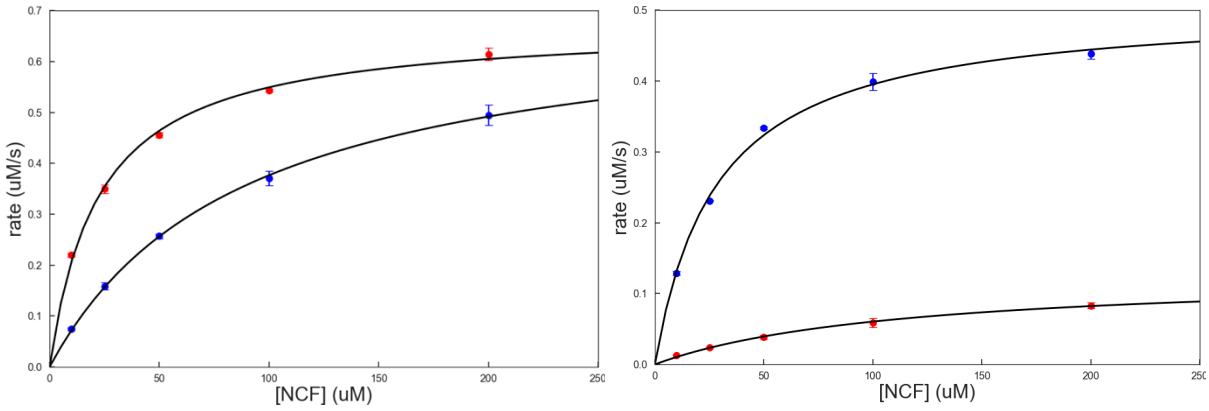

Figure S6: Activity of enzyme before (blue) and after (red) addition of covalent DTNB label for TEM-1 S243C (left) and CTX-M-9 (right). Blue points are unlabeled enzyme, red points are labeled enzyme. Points were taken in triplicate. Fits are to a Michaelis-Menten model.

Table S3. Parameters for Michaelis-Menten model of enzyme activity. Error is the standard deviation from 100 trials of bootstrapping.

	k_{cat} (s^{-1})	K_M (μM)
TEM-1 M182T S243C	354 ± 13	88 ± 5
Labeled TEM-1 M182T S243C	337 ± 9	22 ± 2
CTX-M-9	254 ± 10	28 ± 3
Labeled CTX-M-9	65 ± 8	114 ± 21

Synthetic labeling of TEM-1 residues

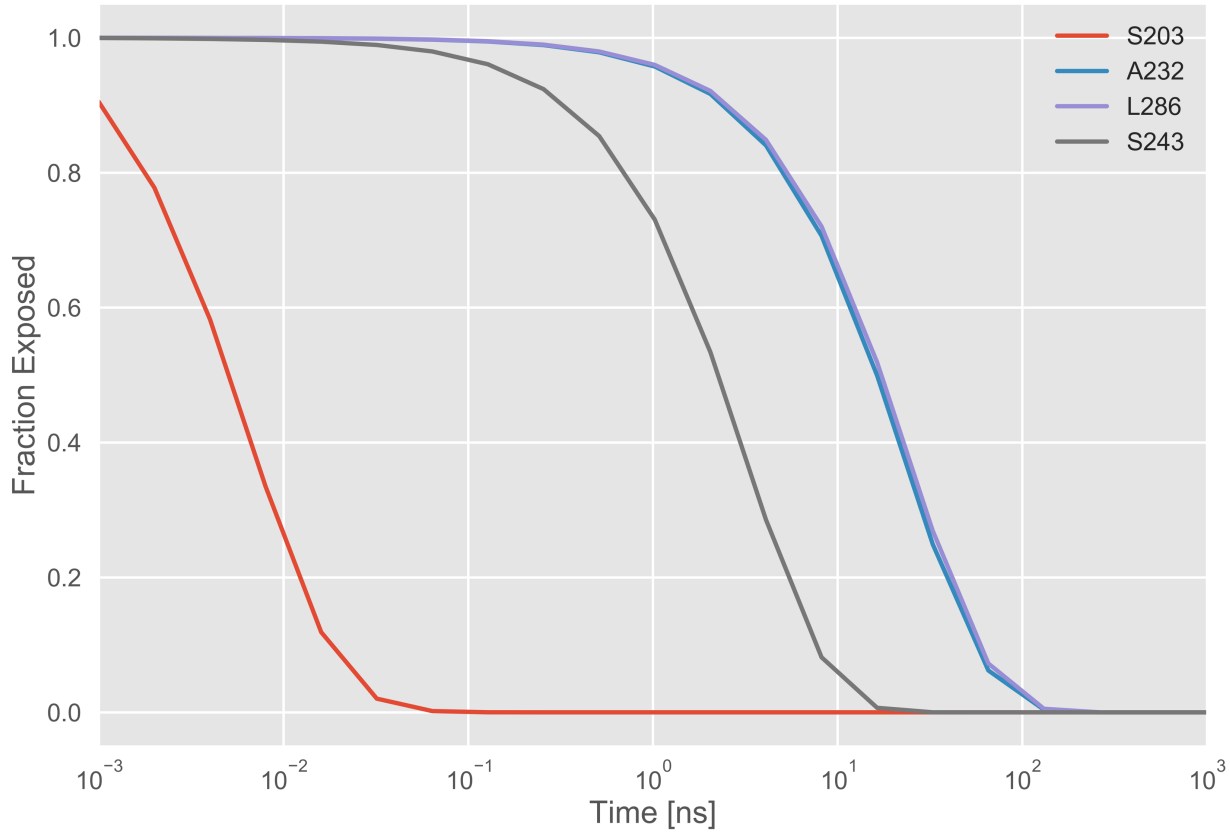

Figure S7: Synthetic labeling traces of various TEM-1 residues indicate the fraction of the population (y-axis) that is expected to be have been exposed to solvent after a particular amount of time (x-axis). The rank order here recapitulates the *in vitro* rates' order reported in (4).

Estimation of druggability of S243 pocket

We used fpocket (5) to estimate the druggability of every frame associated with a microstate where S243 is classified as exposed. We then filtered pockets for S243 gamma oxygen involvement and for the lack of involvement of the active site serine, S70. As noted in the main text, traditional pocket detection algorithms have a tendency to combine this pocket with the active site, as they often form a channel-like connection, despite being geometrically distinct. We expect the druggabilities noted here to be lower bound estimates for druggability, the druggability score was trained on crystal structures of ligands, which are typically adopt a more closed conformation created by contributions of induced fit, whereas in simulation these same pockets are often much more open (6).

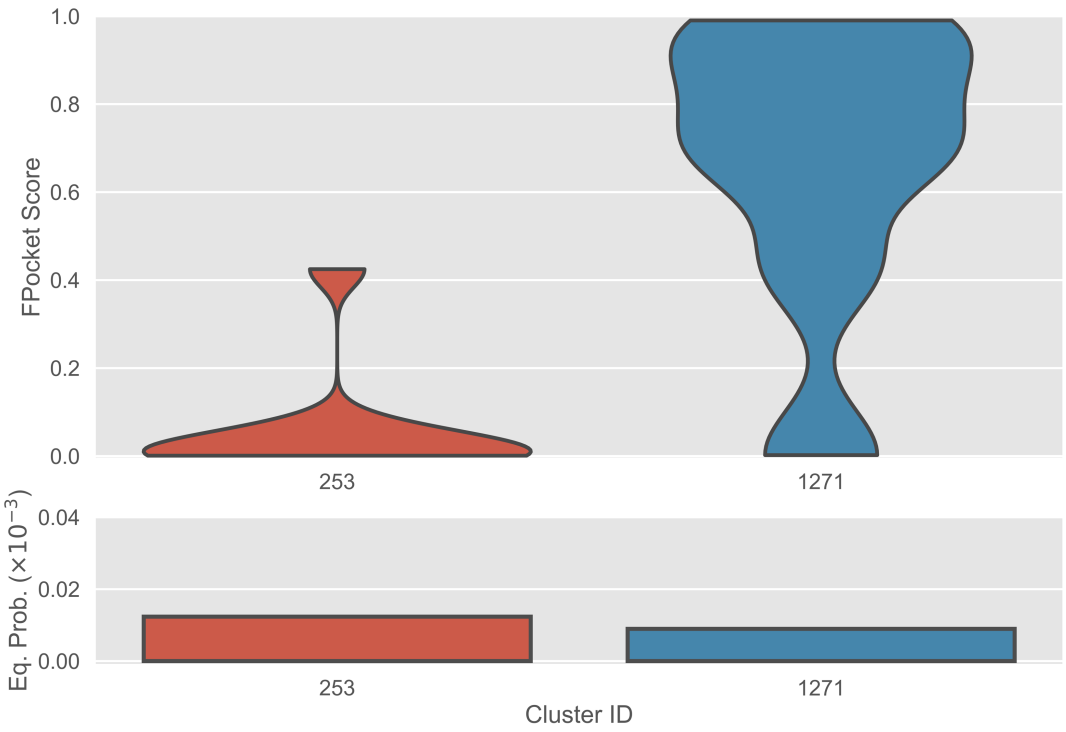

Figure S8: Druggability and equilibrium probabilities for pockets involving S243. *Top*, a violin plot of the distribution of FPocket druggability score for both microstates with exposed S243. *Bottom*, the equilibrium probability of each of those states. These data suggest a minor population of a very-likely druggable conformation (state 1271, blue).

k_{obs} is bounded above by $k_{\mathrm{obs}}^{(\mathrm{EX1})}$ and $k_{\mathrm{obs}}^{(\mathrm{EX2})}$.

As defined in *Methods* of the main text, the observed labeling rates of the three regimes are defined as:

$$k_{\mathrm{obs}} = \frac{k_{\mathrm{op}} k_{\mathrm{int}}[\mathrm{DTNB}]}{k_{\mathrm{op}} + k_{\mathrm{cl}} + k_{\mathrm{int}}[\mathrm{DTNB}]}$$

$$k_{\mathrm{obs}}^{(\mathrm{EX2})} = \frac{k_{\mathrm{op}}}{k_{\mathrm{cl}}} k_{\mathrm{int}}[\mathrm{DTNB}] = K k_{\mathrm{int}}[\mathrm{DTNB}]$$

$$k_{\mathrm{obs}}^{(\mathrm{EX1})} = k_{\mathrm{op}}$$

We want to show that $k_{\mathrm{obs}} < k_{\mathrm{obs}}^{(\mathrm{EX2})}$ and $k_{\mathrm{obs}} < k_{\mathrm{obs}}^{(\mathrm{EX1})}$.

Hypothesis I: $\boldsymbol{k_{\mathrm{obs}} < k_{\mathrm{obs}}^{(\mathrm{EX2})}}$

$$k_{\mathrm{obs}} < k_{\mathrm{obs}}^{(\mathrm{EX2})}$$

$$\frac{k_{\mathrm{op}} k_{\mathrm{int}}[\mathrm{DTNB}]}{k_{\mathrm{op}} + k_{\mathrm{cl}} + k_{\mathrm{int}}[\mathrm{DTNB}]} < \frac{k_{\mathrm{op}}}{k_{\mathrm{cl}}} k_{\mathrm{int}}[\mathrm{DTNB}]$$

$$\frac{1}{k_{\mathrm{op}} + k_{\mathrm{cl}} + k_{\mathrm{int}}[\mathrm{DTNB}]} < \frac{1}{k_{\mathrm{cl}}}$$

$$k_{\mathrm{op}} + k_{\mathrm{cl}} + k_{\mathrm{int}}[\mathrm{DTNB}] > k_{\mathrm{cl}}$$

$k_{\mathrm{op}} + k_{\mathrm{int}}[\mathrm{DTNB}] > 0$, which is true, since each term is greater than zero individually.

Hypothesis II: $\boldsymbol{k_{\mathrm{obs}} < k_{\mathrm{obs}}^{(\mathrm{EX1})}}$

$$k_{\mathrm{obs}} < k_{\mathrm{obs}}^{(\mathrm{EX1})}$$

$$\frac{k_{\mathrm{op}} k_{\mathrm{int}}[\mathrm{DTNB}]}{k_{\mathrm{op}} + k_{\mathrm{cl}} + k_{\mathrm{int}}[\mathrm{DTNB}]} < k_{\mathrm{op}}$$

$$\frac{k_{\mathrm{int}}[\mathrm{DTNB}]}{k_{\mathrm{op}} + k_{\mathrm{cl}} + k_{\mathrm{int}}[\mathrm{DTNB}]} < 1$$

$$k_{\mathrm{int}}[\mathrm{DTNB}] < k_{\mathrm{op}} + k_{\mathrm{cl}} + k_{\mathrm{int}}[\mathrm{DTNB}]$$

$0 < k_{\mathrm{op}} + k_{\mathrm{cl}}$, which is true, since each term is greater than zero individually.

Thus, since $k_{\mathrm{obs}} < k_{\mathrm{obs}}^{(\mathrm{EX2})}$ and $k_{\mathrm{obs}} < k_{\mathrm{obs}}^{(\mathrm{EX1})}$ we can conclude that $k_{\mathrm{obs}} < \min\left\{k_{\mathrm{obs}}^{(\mathrm{EX2})}, k_{\mathrm{obs}}^{(\mathrm{EX1})}\right\}$, i.e. that the EX1 and EX2 observed rates serve as strict upper bounds to the EXX observed rate.

References

1. Pande, V.S., K.A. Beauchamp, and G.R. Bowman. 2010. Everything you wanted to know about Markov State Models but were afraid to ask. Methods. 52: 99–105.

2. Bowman, G.R., V.S. Pande, and F. Noé. 2013. An Introduction to Markov State Models and Their Application to Long Timescale Molecular Simulation. Springer Science & Business Media.

3. Bolen, D.W., and M.M. Santoro. 1988. Unfolding free energy changes determined by the linear extrapolation method. 2. Incorporation of delta G degrees N-U values in a thermodynamic cycle. Biochemistry. 27: 8069–8074.

4. Hart, K.M., C.M.W. Ho, S. Dutta, M.L. Gross, and G.R. Bowman. 2016. Modelling proteins' hidden conformations to predict antibiotic resistance. Nat. Commun. 7: 12965.

5. Schmidtke, P., and X. Barril. 2010. Understanding and predicting druggability. A high-throughput method for detection of drug binding sites. J. Med. Chem. 53: 5858–5867.

6. Bowman, G.R., and P.L. Geissler. 2012. Equilibrium fluctuations of a single folded protein reveal a multitude of potential cryptic allosteric sites. Proc. Natl. Acad. Sci. U.S.A. 109: 11681–11686.